The Faraday resonance of interfacial waves in weakly viscous fluids

D. F. Hill[a)]
Department of Civil and Environmental Engineering, The Pennsylvania State University, 212 Sackett Building, University Park, Pennsylvania 16802

(Received 2 May 2000; accepted 27 September 2001)

The Faraday resonance of interfacial waves in a two-layer, weakly-viscous system in a rectangular domain is presented. A perturbation analysis is pursued and, at the second-order, the scaling of the viscosity results in boundary layer corrections at the solid walls and at the interface. Special attention is paid to the damping in the meniscus region where the interface contacts the side-walls. As a result of the presence of both destabilizing effects (vertical oscillation) and stabilizing effects (viscosity), a threshold condition for instability is determined. The derived analytic results are quite general and prove useful in elucidating the influences of the various boundary layers, as well as the threshold for growth. In an effort to describe the maximum amplitude attained by the resonated wave, a third-order analysis is then presented for the idealized case of equal-depth, inviscid layers, with a rigid-lid condition at the free surface. A balance between cubic nonlinearity and the vertical shaking yields a Landau-type equation for the interfacial wave amplitude. Comparisons with some existing experimental data are made at both orders and indicate very good agreement. © *2002 American Institute of Physics.* [DOI: 10.1063/1.1425846]

I. INTRODUCTION

Succinctly defined by Drazin and Reid,[1] a parametric instability is an instability that occurs when the base flow of a fluid system is periodic in time. Careful tuning of the forcing can yield resonated modes that are either superharmonics or subharmonics of the forcing frequency.

It is this instability that was observed by Faraday[2] when he immersed a vibrating plate in water. Specifically, he noted the presence of subharmonic waves on the free surface. The rigorous explanation of this phenomenon was provided by Benjamin and Ursell.[3] They first noted that a vertically oscillating system is equivalent to a stationary system in the presence of a periodic gravitational field. Then, by linearizing the equations of motion, they reduced the boundary value problem to a form of Mathieu's equation. A concise summary is provided by Drazin and Reid[1] (Sec. 48.2).

An example of a parametric instability driven by nonlinear interactions, rather than periodic vertical acceleration, is the presence of edge waves on sloping boundaries. These trapped modes propagate in the longshore direction and were shown, by Guza and Davis,[4] to be resonated by weakly nonlinear, normally incident surface waves. It has been suggested that edge waves play a role in the development of regularly spaced beach cusps in many coastal areas. A review of parametrically excited surface waves, including both oscillating basins and nonlinear resonance, is given by Miles and Henderson.[5]

It has recently been shown by Hill and Foda[6] that interfacial and internal waves are also susceptible to subharmonic resonance by weakly nonlinear surface waves. It was shown that monochromatic surface waves could resonate two trains of oblique waves at the interface of a two-layer system. Laboratory experiments verified both the first and second-order theoretical predictions for growth and revealed that the interfacial waves would grow in size until they began to break, and subsequently mix fluid across the interface.

Faraday resonance continues to attract the attention of numerous researchers, due in parts to the significance of vertically oscillating flows and to the convenient framework it provides for studies of stability and damping. An example of the former is provided by Foda and Chang,[7] who studied the Faraday resonance of thin viscoelastic layers. This mechanism was offered as an explanation of the short-scale variability of amplification factors observed in the seismic records of many earthquakes. Kumar[8] also studied the Faraday resonance of waves in viscoelastic fluids, noting its potential application as a tool for measurement of rheological properties. Of particular interest were the differences in behavior between viscoelastic and Newtonian fluids.

With regards to stability and damping studies, a wealth of literature exists on the subject of the growth and damping of capillary waves in right circular cylinders. In the damping studies, while the Faraday resonance itself may not always be of primary interest, it is often used as the mechanism for generating the waves whose damping rates are subsequently measured. The convenience of studying temporal growth and decay rates, as opposed to spatial growth and decay rates in a wave channel, has facilitated very precise study of numerous phenomena, including contact line dynamics[9] and the effects of surfactants.[10]

In addition to being ideally suited for experimental studies, the simplicity of the Faraday instability has allowed exploration with several different analytic techniques. For example, straightforward multiple-scales analyses are frequently used in conjunction with solvability conditions in

a)Telephone: 814-863-7305. Electronic mail: dfhill@engr.psu.edu

order to obtain an amplitude evolution equation. Miles,[11] on the other hand, computed the Lagrangian of the system and then used Hamilton's principle to arrive at the evolution equation. More recently, Miles[12] discussed a rather more compact approach that relied upon specification of the surface-wave ''impedance'' in order to arrive at the threshold forcing required for growth.

The current paper considers the Faraday resonance of waves at the interface between two weakly-viscous fluids. Through restriction to weak viscosity, the viscous effects are confined to boundary layers at the solid walls and interface and introduce velocity corrections to the second-order problem. These corrections lead to attenuation of the wave amplitude and a slight frequency shift away from the inviscid value. The damping rates determined in this fashion are, when care is exercised near the interfacial meniscus, identical to those determined by computing the dissipation in the boundary layers.

The competition between the forcing and the damping results in an analytical expression for the critical forcing amplitude necessary for growth. More generally, an amplitude evolution equation of the form,

$$\dot{a} \sim i\alpha a^* + \beta a,$$

where a is the complex amplitude, α a real instability coefficient, and β a complex damping coefficient, is obtained.

While damping in stratified fluids has received wide attention in the past, it has been primarily from the point of view of its effect on surface waves. Dalrymple and Liu,[13] Hsiao and Shemdin,[14] and Piedra-Cueva[15] all considered the damping rates of progressive surface waves due to the viscosity in the lower layer of a two-layer system. These investigations varied in terms of the assumed lower layer rheology and whether or not a boundary layer formulation was employed. The lattermost author explicitly considered side-wall effects, a result of particular relevance to experimental studies. Studies that have specifically focused on internal and interfacial wave damping include those of Schooley and Stewart,[16] Thorpe,[17] and, more recently, Benielli and Sommeria,[18] hereafter referred to as B&S. The first two papers discuss dissipation in side-wall and bottom boundary layers, but for approximate cases only, such as deep layers of equal viscosity. The lattermost paper is of particular interest and significance to the current study as it discusses interfacial Faraday resonance. Throughout the analysis presented herein, therefore, attempts will be made to contrast the current results with those of B&S.

Third-order effects are also considered in the current paper, for a simplified case. It is well known that parametrically excited waves will attain some maximum amplitude, as the frequency of the resonated wave detunes from the forcing frequency. In the context of edge waves, for example, this maximum has been described by Guza and Bowen[19] and Minzoni and Whitham.[20] The derivation of this amplitude is straightforward in principle, but proves to be quite tedious in practice for baroclinic modes. Therefore, restriction is made, for this third-order analysis only, to inviscid layers of equal, but general, depth, with a rigid-lid at the free surface. The result in this case is an evolution equation of the general form,

$$\dot{a} \sim i\alpha a^* + i\lambda a^* a^2,$$

where λ is a nonlinear interaction coefficient.

The results of the current investigation are of interest since the growth and dissipation of interfacial and internal waves play important roles in the dynamics of lakes and coastal and estuarine areas. As illustrated above, the attenuation of surface waves is a topic of great interest. While the attenuation due to lower layer viscosity has been treated in great detail, similar attention has yet to be paid to the transfer of energy, demonstrated by Hill and Foda,[6] from surface waves to the internal wave field.

Another relevant mechanism that has been detailed in a series of papers by Raichlen and Ting[21] and Ting[22,23] is that of forced internal and interfacial waves in rectangular trenches. With the goal of understanding the dynamics of fluid-mud layers in dredged navigation channels, the authors investigated the linear resonance of internal and interfacial waves in finite domains for a variety of conditions. Viscous, viscoelastic, and continuously stratified lower layers were all considered. Whether or not mud waves in these channels could be resonated by parametric instability as well is still an open question.

Finally, the breaking of internal and interfacial waves, both on sloping boundaries and in the fluid interior, has motivated a great deal of research in recent years. This is largely due to the role that this breaking plays in vertical mixing and the horizontal transport of scalars. For example, Ivey and Nokes[24] and Taylor[25] both experimentally investigated the turbulent boundary layer that was generated on a constant slope due to the breaking of critical internal waves. Measurements of the vertical mixing were made and simple dye studies illustrated that this localized process could cause global, or basin-scale, horizontal transport in the form of intrusions of mixed fluid into the interior. Thorpe[17] and McEwan,[26] on the other hand, studied breaking internal waves in the absence of topographic variation. An interesting and very recent numerical study of two-dimensional interfacial Faraday waves by Wright *et al.*[27] is noteworthy as it seems to indicate breaking. By analyzing the oscillations at the interface between two semi-infinite fluids, the authors were able to demonstrate strong deformation and eventual breakup of the interface, suggesting the onset of breaking.

The present results could therefore be used to guide further experiments on internal wave breaking in the fluid interior and the accompanying mixing efficiency. For while the experiments of Hill and Foda[6] were useful in identifying surface waves as a significant source of internal wave energy, the quantification of subsequent mixing due to breaking in the interior proves difficult in the case of progressive waves in a channel. The inevitable mixing along the sloping beach and in the vicinity of the wavemaker will artificially and significantly inflate the overall mixing observed in the channel. On the other hand, standing interfacial waves, excited through Faraday oscillation, provide a straightforward means through which to quantitatively further the study of the breaking process.

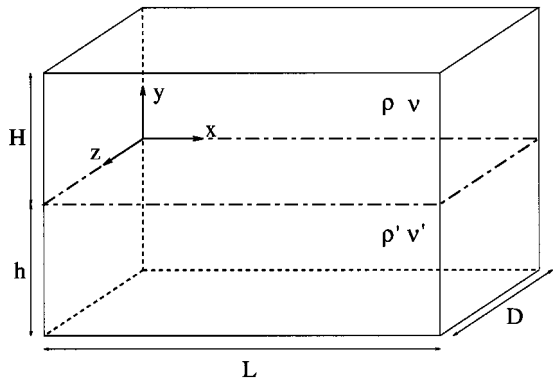

FIG. 1. Schematic of the weakly viscous two-layer fluid system.

II. INSTABILITY FORMULATION

As illustrated in Fig. 1, a layer of depth H, density ρ and viscosity ν overlies a layer of depth h, density ρ', and viscosity ν'. The density ratio $\gamma=\rho/\rho'$ is assumed to be less than unity. The fluid layers are contained in a box with horizontal dimensions L by D. A Cartesian coordinate system is fixed at the interface between the two fluids and at one corner of the box as shown.

The base of the system is assumed to oscillate about its mean position of $y=-h$ with a frequency 2ω and an amplitude of displacement b. With the coordinate system fixed at the interface, thereby oscillating as well, this leads to a modulated gravitational acceleration. The effective gravitational constant is given by

$$g_e=\frac{g}{2}+2\omega^2 b e^{2i\omega t}+\text{c.c.},$$

where c.c. denotes the complex conjugate. Hereafter, the complex conjugate will be understood in expressions for the displacement variables and the velocity potentials.

To describe interfacial wave motion, a small departure of the interface from its equilibrium plane $y=0$ is given by

$$\eta=\frac{a}{2}\cos(k_x x)\cos(k_z z)e^{i\omega t}.$$

The frequency of the wave is ω, exactly one-half the frequency of the oscillating base. Additionally, the amplitude is a, and the wave number vector is given by $\mathbf{k}=k_x\hat{i}+k_z\hat{k}$. The motion of the free surface, in response to this baroclinic mode, is given by the reduced amplitude,

$$\zeta=\frac{a_r}{2}\cos(k_x x)\cos(k_z z)e^{i\omega t}.$$

At this point, it is worth briefly commenting on the response of the interface in the context of the stability of Mathieu's equation. To simplify matters, assume, for the time being, that both layers are inviscid and of equal depth H. Furthermore, assume that the free surface is replaced by a rigid lid and that the waves are two-dimensional ($k_z=0$). These are the same assumptions that will be made in Sec. V. Finally, take the forcing to be at a frequency twice that of the fundamental ($k_x=\pi/L$) mode.

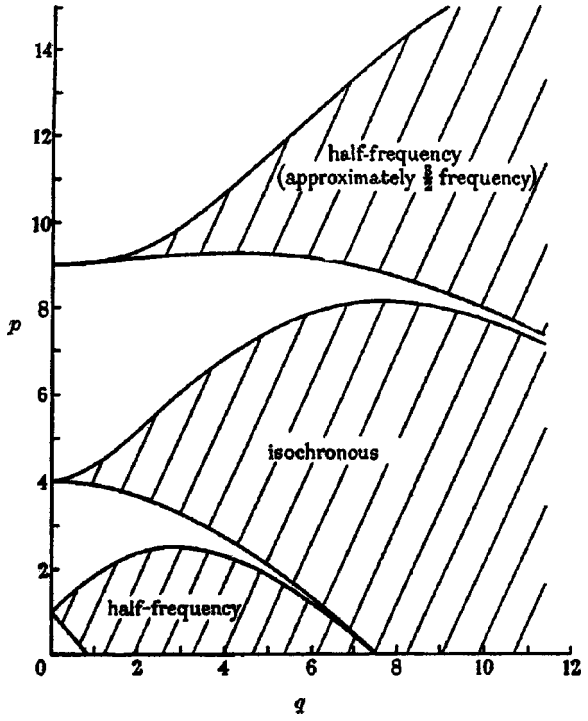

FIG. 2. Stability chart for the solutions of Mathieu's equation. Reprinted from Benjamin and Ursell (Ref. 3) with permission from the Royal Society of London.

Following the analysis and nomenclature of Benjamin and Ursell,[3] and expanding the variables in terms of the complete orthogonal set of eigenfunctions, it can be shown that

$$\frac{d^2 a_m}{dT^2}+[p_m-2q_m\cos(2T)]a_m=0,$$

where $m=1,2,3,\ldots,a_m$ and k_m are the amplitude and wavenumber of eigenfunction m, $T=\omega t$, and

$$p_m=\frac{gk_m(1-\gamma)\tanh(k_m H)}{\omega^2(1+\gamma)},$$

$$q_m=2bk_m\tanh(k_m H)\frac{1-\gamma}{1+\gamma}.$$

Since the forcing is at a frequency twice that of the fundamental free wave, $p_1=1$ by definition. This places the first mode at the center of the subharmonic tongue of the Mathieu stability chart, which is shown in Fig. 2. If q_m is sufficiently large, it is technically possible for the response of the surface to be synchronous, but a quick inspection reveals that, for realistic values of γ and b, $q_m \ll 1$ and the response will be subharmonic. For example, for $\gamma=0.79$, $H=12.5$ cm, $b=3.5$ cm, and $L=26.1$ cm, it is found that $q_1=0.0896$.

There is the slight possibility of higher modes falling within the other tongues of the stability chart, but this is unlikely since the second and third tongues of the stability chart are extremely narrow for $q_m \ll 1$. Because of the nonlinear nature of the dispersion relationship, it is unlikely that higher values of p will be sufficiently close to 4 and 9 so as to place the (p,q) pairs in these tongues. Using the same parameters as in the previous paragraph, (p_2,q_2)

$=(2.20,0.20)$ and $(p_3,q_3)=(3.31,0.30)$. Moreover, and practically speaking, even if this did occur, higher modes tend to be suppressed in dissipative systems.

Returning now to the formulation of the general, weakly-viscous problem, the fluid velocity vectors in both layers are assumed to be the sums of irrotational and rotational parts, so that $\mathbf{u}=(u,v,w)=\nabla\Phi+\mathbf{U}$. Here, Φ is a velocity potential and $\mathbf{U}=(U,V,W)$ is a solenoidal vector. As a result, the equation of continuity in both layers reduces to Laplace's equation,

$$\nabla^2\Phi=0 \quad -h\leqslant y\leqslant H. \tag{1}$$

The momentum equation yields the following two equations for the solenoidal vectors,

$$\mathbf{U}_t-\nu\nabla^2\mathbf{U}=0 \qquad 0\leqslant y\leqslant H, \tag{2}$$

$$\mathbf{U}_t-\nu'\nabla^2\mathbf{U}=0 \qquad -h\leqslant y\leqslant 0. \tag{3}$$

As for boundary conditions, the no slip and no flow conditions require that the fluid velocity vector $\mathbf{u}$ vanish on all solid boundaries,

$$\nabla\Phi+\mathbf{U}=0, \quad y=-h; \quad x=0,L; \quad z=0,D. \tag{4}$$

At the free surface, there are the usual kinematic and dynamic conditions, the latter departing from its familiar form with the addition of the viscous normal stress,

$$\zeta_t=v, \quad y=H, \tag{5}$$

$$\Phi_t+g_e\zeta+2\nu v_y=0, \quad y=H. \tag{6}$$

There is an additional condition at the free surface that arises from the inclusion of viscosity. The condition is that the shear stresses vanish,

$$\rho\nu(u_y+v_x)=\rho\nu(w_y+v_z)=0, \quad y=H. \tag{7}$$

At the interface, there is first the condition of continuity of velocity,

$$\mathbf{u}^+=\mathbf{u}^-, \quad y=0. \tag{8}$$

Note that the $+$ and $-$ superscripts denote quantities in the upper and lower layers, respectively. In addition, there are the equations describing the continuity of shear stress and normal stress at the interface,

$$\gamma\nu(u_y+v_x)^+=\nu'(u_y+v_x)^-, \quad y=0, \tag{9}$$

$$\gamma\nu(w_y+v_z)^+=\nu'(w_y+v_z)^-, \quad y=0, \tag{10}$$

$$\gamma(\Phi_t+g_e\eta-2\nu v_y)^+=(\Phi_t+g_e\eta-2\nu' v_y)^-, \quad y=0. \tag{11}$$

Next, the following scalings are adopted. Note that the asterisks denote dimensionless quantities and that the asterisks are subsequently dropped,

$$t^*=t\sqrt{g|\mathbf{k}|}, \quad \omega^*=\frac{\omega}{\sqrt{g|\mathbf{k}|}}, \quad \Phi^*=\frac{\Phi}{b\sqrt{g/|\mathbf{k}|}},$$

$$\mathbf{U}^*=\frac{\mathbf{U}}{b\sqrt{g|\mathbf{k}|}}, \quad (\nu^*,\nu'^*)=\frac{|\mathbf{k}|^2(\nu,\nu')}{\epsilon^{*2}\sqrt{g|\mathbf{k}|}},$$

$$(k_x^*,k_z^*)=\frac{(k_x,k_z)}{|\mathbf{k}|},$$

$$\epsilon^*=\frac{2b\omega^2}{g}, \quad \eta^*=\frac{\eta}{b}, \quad a^*=\frac{a}{b},$$

$$(x^*,y^*,z^*,H^*,h^*,L^*,D^*)=|\mathbf{k}|(x,y,z,H,h,L,D).$$

The parameter ϵ quantifies the acceleration due to the vertical oscillation relative to gravity and is assumed to be much less than unity. Note that the viscosities of both layers have been scaled as ϵ^2. Recalling that the thickness of an oscillatory boundary layer goes by the square root of the viscosity, this is therefore equivalent to scaling the boundary layer thicknesses as $O(\epsilon)$. This weak scaling greatly simplifies the boundary conditions, as many terms are removed to higher orders.

III. INSTABILITY SOLUTION

To solve the problem, the velocity potential is first expanded in a power series of ϵ, so that

$$\Phi=\phi(y,\tau)\cos(k_x x)\cos(k_z z)e^{i\omega t}, \tag{12}$$

with $\phi=\phi_0+\epsilon\phi_1+\cdots$. Note that $\tau=\epsilon t$ is the slow time scale that will govern the growth of the internal waves.

A. $O(1)$

At this order, a homogeneous boundary value problem for ϕ_0 is obtained. Both the modified gravitational effects and the viscous effects are absent. The solutions are well known (e.g., Lamb,[28] Article 231).

$$\phi_0=\frac{ia(\tau)}{2}\left[\left(\frac{\omega\,\mathrm{cth}(h)}{\gamma}-\frac{1-\gamma}{\gamma\omega}\right)\mathrm{ch}(y)+\omega\,\mathrm{sh}(y)\right], \tag{13}$$

$$\phi_0'=\frac{i\omega a(\tau)}{2\,\mathrm{sh}(h)}\mathrm{ch}(y+h), \tag{14}$$

$$\omega^2=\frac{[\mathrm{cth}(h)+\mathrm{cth}(H)]-\sqrt{[\mathrm{cth}(h)+\mathrm{cth}(H)]^2-4(1-\gamma)[\gamma+\mathrm{cth}(h)\mathrm{cth}(H)]}}{2[\gamma+\mathrm{cth}(h)\mathrm{cth}(H)]}.$$

In the above, note that cth, ch, and sh are used for brevity to represent coth, cosh, and sinh. For the no flow boundary conditions on the side walls to be satisfied, the wave number components must take on the values,

$$k_x=\frac{n\pi}{L},\quad k_z=\frac{m\pi}{D},$$

where n and m are positive integer values. Since the scaled wave number vector has a magnitude of unity, the mode numbers satisfy

$$(n\pi/L)^2+(m\pi/D)^2=1. \tag{15}$$

B. Boundary layer correction

With these solutions in hand, the leading-order boundary layer corrections at the solid walls and at the interface can be found. Because of the scaling of the viscosity, Eqs. (2), (3) demand a fast coordinate in the direction normal to the boundary under consideration. If x_N is the coordinate normal to a wall, the positive direction being *into* the fluid, then the appropriate fast coordinate is $\xi=x_N/\epsilon$. Note that at the interface, since there are two boundary layers, there are two fast coordinates, one pointing into the upper layer, and one into the lower layer.

As detailed by Mei and Liu,[29] the diffusion equations for the rotational velocity components *tangential* to the boundary are solved for each boundary layer. In the cases of the solid walls, they are solved subject to (4), while in the cases of the interfacial boundary layers, they are solved subject to (8)–(10). For all boundary layers, use is also made of the condition that the corrections vanish as $\xi\to\infty$. The final step is to integrate continuity in order to obtain the component of the rotational velocity *normal* to each boundary. Due to the boundary layer structure, this normal component is $O(\epsilon)$, while the tangential components and Φ are all $O(1)$.

For the current problem, there are a total of eleven boundary layers (one at the bottom, two at the interface, and eight at the side walls) which must be accounted for. Solution for these terms, while lengthy, is straightforward. As an example, in the bottom boundary layer, the three components of the rotational velocity vector are found to be

$$U=\frac{i\omega a(\tau)k_x}{2\,\mathrm{sh}(h)}\exp\left[-(1+i)\sqrt{\frac{\omega}{2\nu'}}\xi\right]\sin(k_xx)\cos(k_zz),$$

$$W=\frac{i\omega a(\tau)k_z}{2\,\mathrm{sh}(h)}\exp\left[-(1+i)\sqrt{\frac{\omega}{2\nu'}}\xi\right]\cos(k_xx)\sin(k_zz),$$

$$V=\frac{(1+i)\omega a(\tau)}{2\,\mathrm{sh}(h)}\sqrt{\frac{\nu'}{2\omega}}\times\exp\left[-(1+i)\sqrt{\frac{\omega}{2\nu'}}\xi\right]\cos(k_xx)\cos(k_zz).$$

The solutions for the other boundary layers follow similarly and are not presented here.

C. $O(\epsilon)$

At this order, an inhomogeneous problem for ϕ_1 is obtained. Specifically, the boundary conditions now contain linear forcing terms due to the viscous boundary layer corrections and the vertical oscillation. In addition, terms allowing for the slow modulation of the wave amplitude are present.

Since this problem is inhomogeneous and the homogeneous problem had a nontrivial solution, it is necessary to apply an orthogonality condition. This is known as the Fredholm alternative (e.g., Garabedian[30]) and is accomplished by applying Green's Theorem to ϕ_0^* and ϕ_1. For example,

$$\int_V(\phi_0^*\nabla^2\phi_1-\phi_1\nabla^2\phi_0^*)\,dV=\int_S\left(\phi_0^*\frac{\partial\phi_1}{\partial n}-\phi_1\frac{\partial\phi_0^*}{\partial n}\right)dS, \tag{16}$$

where the V and S denote volume and surface, respectively. Noting that $\nabla^2\phi_0^*=\nabla^2\phi_1=0$ and $\phi_{0_n}^*=0$ at all solid boundaries, we can apply this to the upper and lower layers, yielding

$$0=\int_{S_w}(\phi_0^*\phi_{1_n})\,dS+\int_{S_{\mathrm{fs}}}(\phi_0^*\phi_{1_y}-\phi_1\phi_{0_y}^*)\,dS+\int_{S_i}(-\phi_0^*\phi_{1_y}+\phi_1\phi_{0_y}^*)\,dS, \tag{17}$$

$$0=\int_{S_w}(\phi_0^*\phi_{1_n})\,dS+\int_{S_b}-\phi_0^*\phi_{1_y}\,dS+\int_{S_i}(\phi_0^*\phi_{1_y}-\phi_1\phi_{0_y}^*)\,dS. \tag{18}$$

In these equations, S_w denotes the wall surfaces, S_{fs} the free surface, S_b the bottom, and S_i the interface. The subscript n denotes differentiation along the *outward* normal direction.

The final step is to combine the equations, specifically in the form $\gamma(17)+(18)$, and substitute in the homogeneous and inhomogeneous boundary conditions. In subsequently evaluating the integrals, care must be exercised at the interface. Specifically, the region of overlap between the interfacial boundary layers and the side wall boundary layers is of interest. As discussed by Mei and Liu,[29] and as illustrated in Fig. 3, V in the interfacial boundary layers varies in magnitude from $O(\epsilon)$ at the edges of the side wall layers to $O(1)$ at the side walls themselves. It is this contribution, easily overlooked when employing a Poincaré boundary layer formulation, that was identified as the source of the discrepancy found by Ursell,[31] who computed different values of damping by adding up boundary layer dissipation and by computing the rate of pressure working from the inviscid interior to the boundary layers.

To clarify this with an example, consider the results of Keulegan,[32] who computed the damping of standing surface waves in a basin of depth H, length L, and breadth B. Adding up the dissipation in the boundary layers, he found that the dimensional damping rate for a two-dimensional, first-mode wave ($k_x=\pi/L\equiv k, k_z=0$) was given by

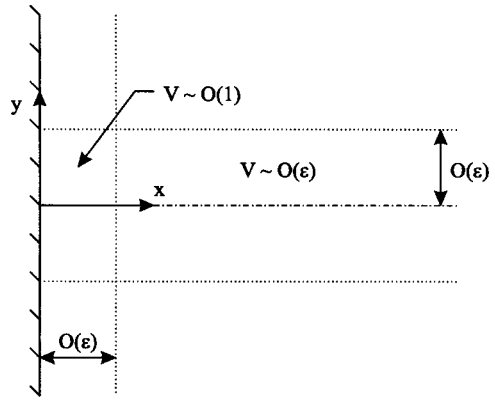

FIG. 3. Closeup of the $x=0$ wall showing the region of overlap between the interfacial and side-wall boundary layers.

$$\sqrt{\frac{\nu\omega}{2}}\left[\frac{1}{B}+\frac{1}{L}+\frac{k(1-2H/L)}{\mathrm{sh}(2kH)}\right]. \tag{19}$$

If the Poincaré boundary layer method of Mei and Liu[29] and the current author is used instead, but the meniscus region is overlooked, the damping will be underpredicted as

$$(1-i)\ \sqrt{\frac{\nu\omega}{2}}\left[-\frac{1}{L}+\frac{k(1-2H/L)}{\mathrm{sh}(2kH)}\right],$$

where the $(1-i)$ factor reinforces that the frequency shift is also obtained. It is only upon inclusion of the meniscus region that the correct result (19) is recovered.

In summary, the boundary layer method of the present analysis and the energy methods of previous analyses yield the same result *only* if the former technique pays careful attention to the damping in the meniscus region. Neither method, however, sufficiently accounts for the discrepancies between theory and experiment noted by Keulegan.[32] Such discrepancies are most likely due to surface tension or some other physical mechanism not considered in that or the current study.

For the current problem, lengthy manipulation of (17) and (18) eventually reveals the exponential growth/decay of the wave amplitude,

$$a\sim e^{\delta\tau}, \tag{20}$$

$$\delta=\mathrm{Re}(\beta)\pm\sqrt{\alpha^2-[\mathrm{Im}(\beta)]^2}. \tag{21}$$

In this expression, α is a positive, real-valued instability coefficient and β is a complex-valued damping coefficient. The forms of these coefficients are quite lengthy and are provided in the Appendix. Of particular note, β can be written as

$$\beta=\beta_b+\beta_i+\beta_m+\beta_{uw}+\beta_{lw},$$

where the individual terms represent damping in the bottom boundary layer, the interfacial layers, the meniscus region, the upper side-walls and the lower side-walls. As will be demonstrated in the following section, it is useful to have the damping broken up into these separate contributions so that a physical understanding of the dominant damping process can be readily obtained. Finally, from (21), the following threshold condition for internal wave growth is readily derived:

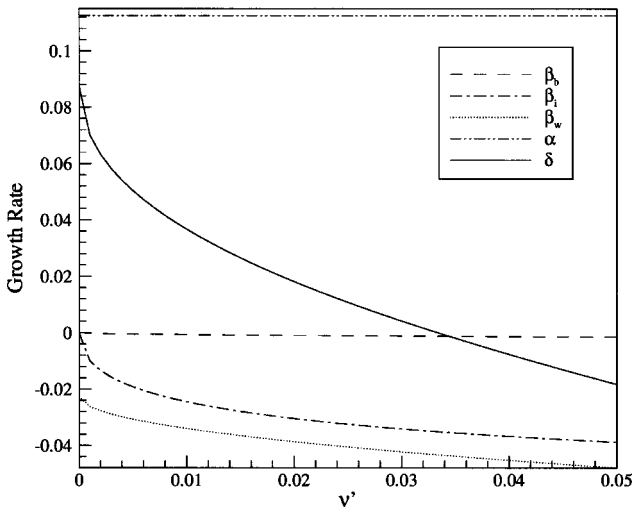

FIG. 4. Variation of damping and instability terms with lower layer viscosity. $H=h=2$, $n=m=1$, $L=D=4.44$, $\nu=0.05$, $\gamma=0.9$.

$$\alpha^2>|\beta|^2. \tag{22}$$

IV. INSTABILITY RESULTS

The analytic results for the damping can be quickly verified by considering the asymptotic limit of no upper layer. By letting $H\to\infty$, $\gamma\to 0$, and $\nu\to 0$, the result of Keulegan[32] discussed in the previous section is indeed recovered.

Next, the variation of the scaled growth rate with the dimensionless parameters can be investigated with (21). Note that the sheer number of parameters coupled with fact that many are related through the dispersion relationship can make interpretation of the trends somewhat difficult.

The most easily understood influence is that of fluid viscosity. This is because viscosity affects neither the leading-order dispersion relationship nor the instability coefficient. Figure 4 illustrates the influence of the lower layer viscosity. The damping rates of the various boundary layers, as well as the instability coefficient (α) and net growth rate (δ) are plotted. Note that, for the sake of clarity, all of the damping associated with the side-walls, including the meniscus term, has been lumped into a single coefficient, i.e.,

$$\beta_w=\beta_m+\beta_{uw}+\beta_{lw}.$$

The obvious result is that the growth rate of the wave decreases with increasing viscosity. If the viscosity is large enough, the instability of the vertical oscillation is suppressed and the internal wave is damped instead. Since the lower layer is relatively deep in this example, the damping due to the bottom boundary layer is very small and the bulk of the damping comes from the interfacial and side-wall boundary layers. The influence of upper layer viscosity on the various terms is similar, but not quite as severe. This is a consequence of having a no-shear rather than a no-slip condition at the free surface.

The dependence upon the lower layer depth is examined in detail in Fig. 5. Clearly, the growth rate of the internal waves diminishes as the lower layer becomes shallow. This is due primarily to the increasing significance of damping in

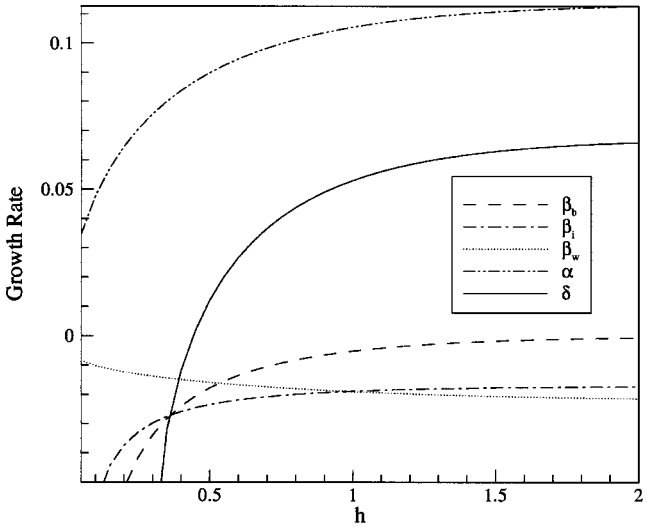

FIG. 5. Variation of damping and instability terms with lower layer depth. $H=2$, $n=m=1$, $L=D=4.44$, $\nu=\nu'=0.01$, $\gamma=0.9$.

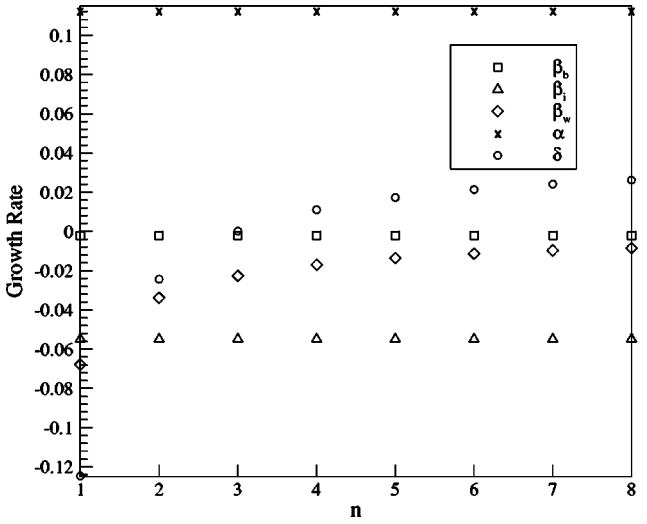

FIG. 6. Variation of growth rate with mode number. $H=h=2$, $\gamma=0.9$, $m=n$, $L=D=\sqrt{2}\pi n$, $\nu'=\nu=0.1$.

the bottom boundary layer, as can be seen in the plot of β_b. If the lower layer becomes shallow enough, the instability of the waves is once again suppressed and there will be no growth.

The relative influence of the side wall damping can be observed by letting the domain containing the waves become large compared to the wavelength. While this does not change the *amount* of energy dissipation in the side wall boundary layers, this amount as a percentage of the total wave energy in the domain will asymptote to zero. An alternative way of thinking about this is to note that the volume of fluid in the side-wall boundary layers will become negligible compared to the volume of the domain. For the sake of simplicity, consider a square box ($D=L$) having equal modes in the two horizontal directions ($m=n$). From (15), therefore, the dimension of the box and the mode number are related by $L=\sqrt{2}\pi n$. Finally, assume that the two layers have the same viscosity ($\nu'=\nu$).

Figure 6 details the damping and instability terms as functions of the mode number *n*. Note that since the domain is increasing in size accordingly, the wavelength of the waves is not changing. Rather, the size of the domain is simply increasing to accommodate more wavelengths. Therefore, the waves are not becoming any shallower or deeper and there is, as expected, no variation seen in either the interfacial or the bottom boundary layer damping. However, note that the effect of the side-wall damping dies off fairly rapidly as the domain becomes larger. Depending upon the value of the viscosity, the first few modes may actually be suppressed, as is the case in this example.

To lend some physical insight to these results, it is useful to briefly consider some dimensional results consistent with laboratory scales. Consider a box of length $L=40\,\mathrm{cm}$ and width $D=60\,\mathrm{cm}$. Assume that a 20 cm layer of fresh water ($\rho=1000\,\mathrm{kg/m^3}$, $\nu=10^{-6}\,\mathrm{m^2/s}$) overlies a 20 cm layer of salt water ($\nu'=10^{-6}\,\mathrm{m^2/s}$) of some density ρ'. The forcing amplitude is taken to be $b=2.5\,\mathrm{cm}$. Figure 7 details, as a function of γ, the frequency and growth rate for several (n,m) pairs. Note that the slow, scaled growth rate δ has now been converted back to its fast, dimensional equivalent. The *e*-folding time constants are seen to be on the order of half a minute, confirming that the Faraday resonance of interfacial waves should be readily observable in the laboratory.

Indeed, a comparison can now be made with the numerical and laboratory results of B&S. While they focused primarily on internal wave Faraday resonance, they do present some limited data on interfacial Faraday experiments. In particular, Fig. 4 of their paper presents the exponential growth of waves at the interface between kerosene and water. The parameters are $\rho=790\,\mathrm{kg/m^3}$, $\rho'=1000\,\mathrm{kg/m^3}$, $\nu=1.6\times10^{-6}\,\mathrm{m^2/s}$, $\nu'=1\times10^{-6}\,\mathrm{m^2/s}$, $L=0.261\,\mathrm{m}$, $D=0.096\,\mathrm{m}$, $h=H=0.125\,\mathrm{m}$, $n=1$, and $b=0.035\,\mathrm{m}$. Their measurements indicate a growth rate of $\delta=0.104\,\mathrm{s^{-1}}$, but their calculations overpredict the growth rate as being $\delta=0.119\,\mathrm{s^{-1}}$. In contrast, the current formulation (21) predicts a growth rate of $0.1046\,\mathrm{s^{-1}}$. B&S ascribe the difference between their measurements and predictions to wetting effects on the sidewalls and point out that the discrepancy increases with mode number (Table I). While the current model shows a similar increase in error with mode number, it appears to be a substantial improvement to the prediction of damping of interfacial waves. In addition, the analytic expression obtained is completely general, allowing for layers of different depths and viscosities, as well as a free surface.

Finally, the threshold condition for growth (22) can be investigated for the current example. This condition proves to be of particular use from a design point of view, facilitating the proper selection of γ, as well as the appropriate forcing amplitude and frequency. For the same dimensional parameter values used in generating Fig. 7, the critical forcing amplitude b_{crit}, i.e., the minimum amplitude required for growth, is shown in Fig. 8.

V. EQUILIBRIUM FORMULATION

To describe the equilibrium of the resonated waves, the effects of nonlinear detuning must be included. To prevent

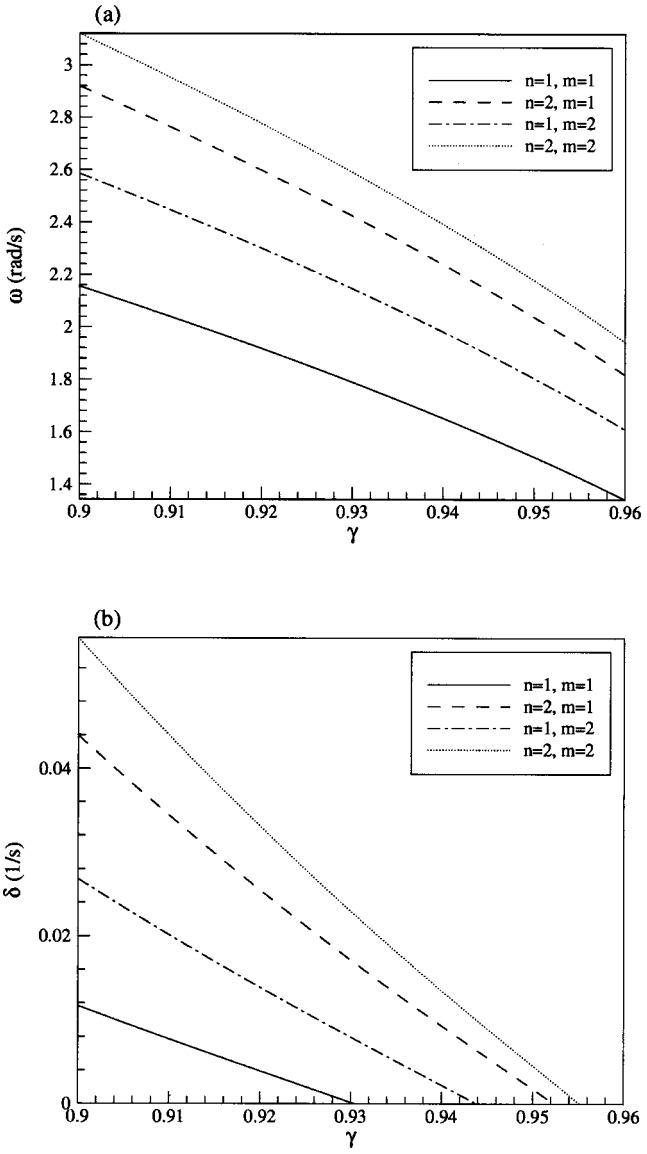

FIG. 7. Dimensional frequencies (a) and growth rates (b) as functions of density ratio and mode numbers. $\rho=1000\ \mathrm{kg/m^3}$, $\nu=\nu'=10^{-6}\ \mathrm{m^2/s}$, $L=40$ cm, $D=60$ cm, $h=H=20$ cm, $b=2.5$ cm.

the results of this section from being obscured by algebraic complexity, two steps will be taken. First, the solution procedure, which is well-known and rooted in perturbation techniques, will be presented in summary fashion only. For a detailed overview (for the case of edge waves) the reader is referred to, e.g., Minzoni and Whitham.[20]

Second, several simplifying assumptions will be made for the current example. Specifically, two-dimensional ($k_z=0$) standing waves between inviscid layers of equal depth (H) will be considered. Additionally, a rigid-lid condition will be assumed at the free surface. Finally, it proves to be convenient to pursue the analysis with dimensional variables. Hence, all of the variables in this and the following sections are assumed to be dimensional.

TABLE I. Comparison of measured and calculated damping rates. Data are from Benielli and Sommeria (Ref. 18). $L=0.261$ m, $D=0.096$ m, $H=h=0.125$ m, $\gamma=0.79$, $\nu=1.6\times10^{-6}\ \mathrm{m^2/s}$, $\nu'=1.0\times10^{-6}\ \mathrm{m^2/s}$.

Mode number n	1	2
β ($\mathrm{s^{-1}}$) (meas. by B&S)	4.6×10^{-2}	7.3×10^{-2}
β ($\mathrm{s^{-1}}$) (calc. by B&S)	3.1×10^{-2}	4.2×10^{-2}
β ($\mathrm{s^{-1}}$) (calc. by Hill)	4.50×10^{-2}	6.64×10^{-2}

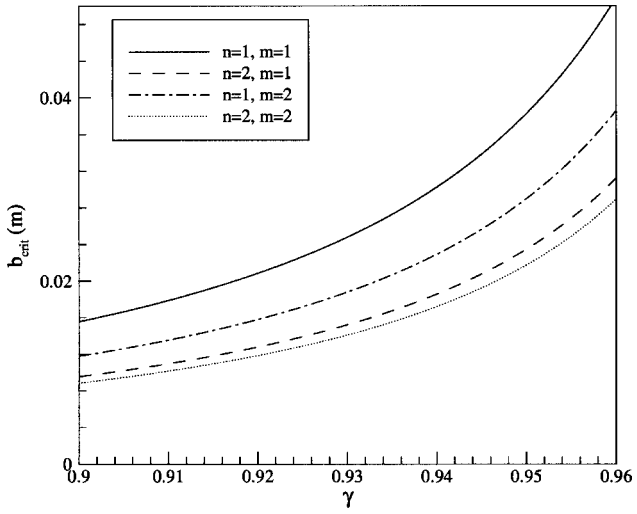

FIG. 8. Critical forcing amplitude as a function of density ratio and mode numbers. $\rho=1000\ \mathrm{kg/m^3}$, $\nu=\nu'=10^{-6}\ \mathrm{m^2/s}$, $L=40$ cm, $D=60$ cm, $h=H=20$ cm.

As before, Laplace's equation holds in both layers and no-flow conditions must be satisfied at the solid boundaries $y=\pm H$ and $x=0, L$. The nonlinear kinematic and dynamic interfacial boundary conditions are Taylor-expanded around $y=0$ to yield

$$\Phi_y^+ - \eta_t = \Phi_x^+\,\eta_x - \eta\Phi_{yy}^+ + \eta\,\eta_x\Phi_{xy}^+ - \tfrac{1}{2}\eta^2\Phi_{yyy}^+, \tag{23}$$

$$\Phi_y^- - \eta_t = \Phi_x^-\,\eta_x - \eta\Phi_{yy}^- + \eta\,\eta_x\Phi_{xy}^- - \tfrac{1}{2}\eta^2\Phi_{yyy}^-, \tag{24}$$

$$\begin{aligned}\gamma[\Phi_t^+ + g_e\eta] - \Phi_t^- - g_e\eta &= \eta\Phi_{ty}^- + \frac{1}{2}(\Phi_x^{-2} + \Phi_y^{-2}) - \gamma\eta\Phi_{ty}^+ - \frac{\gamma}{2}(\Phi_x^{+2} + \Phi_y^{+2}) \\ &\quad + \frac{\eta}{2}[\,\eta\Phi_{ty}^- + \Phi_x^{-2} + \Phi_y^{-2} - \gamma\eta\Phi_{ty}^+ \\ &\quad - \gamma(\Phi_x^{+2} + \Phi_y^{+2})]_y\,.\end{aligned} \tag{25}$$

VI. EQUILIBRIUM SOLUTION

Following the line of reasoning of Minzoni and Whitham[20] and Mei[33] (Sec. 11.4), the orders of magnitude of the wave amplitude and the forcing amplitude are taken to be A and B, respectively. Postulating an equilibrium between the cubic terms, which are $O(A^3)$, and the forcing terms, which are $O(AB)$, implies that, at equilibrium, $A\sim B^{1/2}$. Thus, the following orderings are adopted:

$$\Phi = B^{1/2}\phi_{01}\cos(kx)e^{i\omega t} + B\phi_{12}\cos(2kx)e^{2i\omega t} + B^{3/2}\phi_{21}\cos(kx)e^{i\omega t},$$

$$\eta = B^{1/2}\eta_{01}\cos(kx)e^{i\omega t} + B\eta_{12}\cos(2kx)e^{2i\omega t} + B\eta_{10} + B^{3/2}\eta_{21}\cos(kx)e^{i\omega t},$$

$$g_e = \frac{g}{2} + B2\omega^2 b e^{2i\omega t}.$$

In the dual subscript notation being used here, e.g., ϕ_{pq}, the first index refers to the *order* of the term. The second index refers to the frequency of the term, i.e., $e^{iq\omega t}$.

A. $O(B^{1/2})$

At this order, the linear solution for the interfacial wave, which satisfies the no flow boundary conditions at $y=\pm H$, is found to be (e.g., Lamb,[28] Article 231),

$$\phi_{01}^{+} = \frac{-i\omega a}{2k\,\mathrm{sh}(kh)}\mathrm{ch}[k(y-H)],$$

$$\phi_{01}^{-} = \frac{i\omega a}{2k\,\mathrm{sh}(kh)}\mathrm{ch}[k(y+H)],$$

$$\eta_{01} = \frac{a}{2},$$

$$\omega^2 = gk\frac{1-\gamma}{1+\gamma}\mathrm{th}(kH).$$

B. $O(B)$

Next, the quadratic self-interaction of ϕ_{01} will force both a bound superharmonic, i.e., a Stokes wave, as well as a steady ''set-down'' of the interface. Note that the vertical oscillation is still not felt. The superharmonic is readily shown to have the following solution:

$$\phi_{12}^{+} = \frac{i\omega a^2(1-\gamma)}{32(1+\gamma)\mathrm{sh}^4(kH)}\left[-3-\frac{4}{1-\gamma}\mathrm{sh}^2(kH)\right]\times\mathrm{ch}[2k(y-H)],$$

$$\phi_{12}^{-} = \frac{-i\omega a^2(1-\gamma)}{32(1+\gamma)\mathrm{sh}^4(kH)}\left[-3+\frac{4\gamma}{1-\gamma}\mathrm{sh}^2(kH)\right]\times\mathrm{ch}[2k(y-H)],$$

$$\eta_{12} = \frac{ka^2(1-\gamma)\mathrm{ch}(kH)}{16(1+\gamma)\mathrm{sh}^3(kH)}[2\,\mathrm{ch}^2(kH)+1].$$

By letting $\gamma\to 0$ (i.e., no upper layer), note that the familiar surface-wave solution for the Stokes wave is recovered.

The ''zeroth'' harmonic, on the other hand, is easily determined from the dynamic boundary condition and is given by

$$\eta_{10} = \tfrac{1}{8}\omega^2|a|^2[1+\mathrm{cth}^2(kH)]\cos(2kx) - \frac{k|a|^2}{4\,\mathrm{sh}(2kH)}\frac{1-\gamma}{1+\gamma}.$$

Note in particular the spatially periodic contribution, which is absent for the case of progressive waves (e.g., Dean and Dalrymple,[34] Sec. 11.2.4).

C. $O(B^{3/2})$

Finally, at the third-order, there is an inhomogeneous problem for the fundamental harmonic ϕ_{21}. Forcing terms on the right-hand sides of the interfacial boundary conditions originate from cubic self-interactions of the first-order solutions (ϕ_{01},η_{01}), quadratic interactions between the first-order solutions and the second-order solutions $(\phi_{12},\eta_{12},\eta_{10})$, and the vertical shaking. As before, since the homogeneous problem had a nontrivial solution, the amplitude is allowed to be a slowly-varying function of time. The application of solvability conditions (17), (18) to the two layers leads to the following evolution equation:

$$\frac{da}{dt} = \frac{ib\omega^3}{g}a^* + i\lambda a^* a^2, \tag{26}$$

where the nonlinear interaction coefficient is given by

$$\lambda = -\frac{\omega k^2}{256(1+\gamma)^2\,\mathrm{sh}^4(kH)\mathrm{ch}^2(kH)}[(1+\gamma)^2\,\mathrm{ch}(6kH) - (1-\gamma)(2-\gamma)6\,\mathrm{ch}(4kH) - (7\gamma^2-10\gamma+7)\times\mathrm{ch}(2kH)+6(1-\gamma)(4\gamma-3)]. \tag{27}$$

Thus, initially, when the wave amplitude is small, the second term on the right-hand side vanishes and the exponential growth rate of the previous section is recovered, subject to the simplifying assumptions made in this section. More generally, the evolution equation can be integrated numerically in order to determine the slow evolution of the phase and amplitude of the wave.

VII. EQUILIBRIUM RESULTS

Figure 9 illustrates this evolution, along with the phase-plane diagram, for the $n=1$, $b=0.035$ m case of B&S. For the case of exact subharmonic resonance, their experiments indicate a maximum amplitude of approximately 4 cm. Their calculations, based in part upon the results of Sekerzh-Zen'kovich,[35] predict that the maximum amplitude can be given by

$$a_{\max} = \frac{4\omega}{k}\sqrt{\frac{b}{2g}}\frac{1+\gamma}{\sqrt{1+\gamma^2}}, \tag{28}$$

which, for the current example, yields 7.34 cm.

The current analysis proves to be very similar, yielding a prediction of 6.76 cm for the maximum amplitude. Some care should be taken in comparing this number to experimental data. Due to second-order Stokes-wave contributions, the maximum interfacial displacement will deviate noticeably from $|a|$. Specifically, observations of the interface at an antinode such as $x=0$ will reveal a sharp crest and a flat trough. The current calculations predict a maximum *crest* elevation of 7.14 cm.

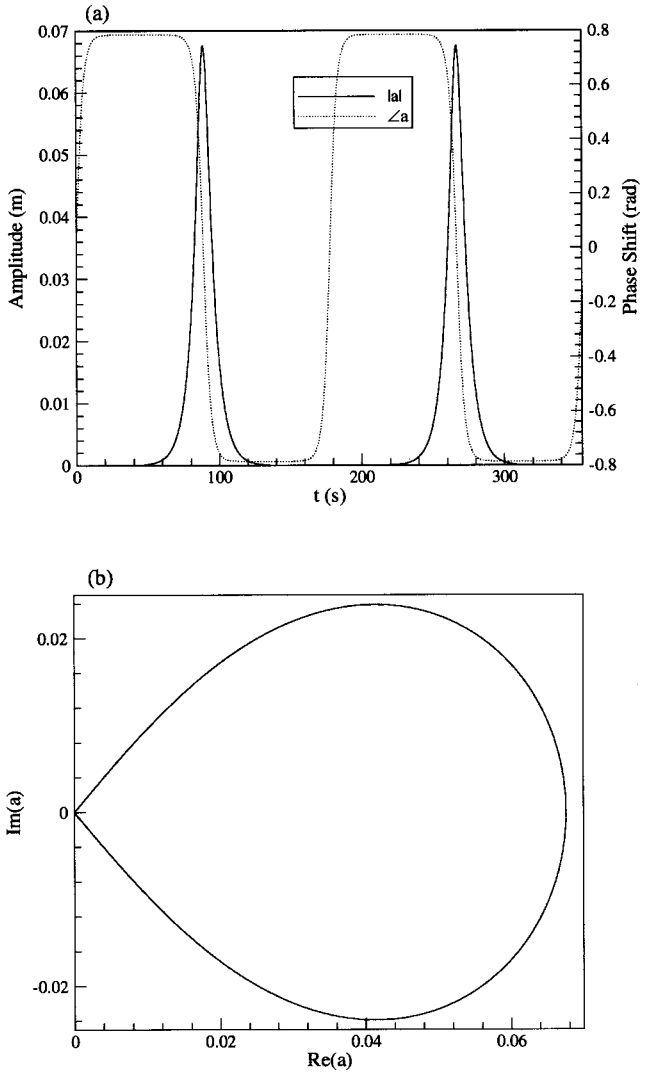

FIG. 9. Evolution of amplitude and phase (a), and phase-plane diagram (b) for $H=12.5$ cm, $\gamma=0.79$, $L=26.1$ cm, $n=1$, $b=3.5$ cm, $\nu=\nu'=0$ m^2/s.

The success of the current analysis in reproducing observations can be substantially improved if viscosity is retained. In this case, the evolution equation is given by

$$\frac{da}{dt}=\frac{ib\omega^3}{g}a^*+\beta a+i\lambda a^*a^2, \tag{29}$$

where the damping coefficient from Sec. III must be modified to account for the rigid lid at the free surface. For the parameter values of B&S being considered here, this yields $\beta=-0.0466(1+i)\,s^{-1}$. Figure 10 clearly demonstrates, for these values, the saturation of the wave amplitude at a value of 3.89 cm. This corresponds to a maximum crest elevation of 4.49 cm which is in very good agreement with their observations.

The simplicity and generality of (26) allow for easy exploration of the results. One trend of interest is the variation in maximum amplitude with mode number. It is commonly held that fundamental ($n=1$) modes are the most unstable and will resonate to larger amplitudes than higher modes. As indicated by Fig. 11, however, this is not the case. Rather, there is an initial increase and then decrease in maximum

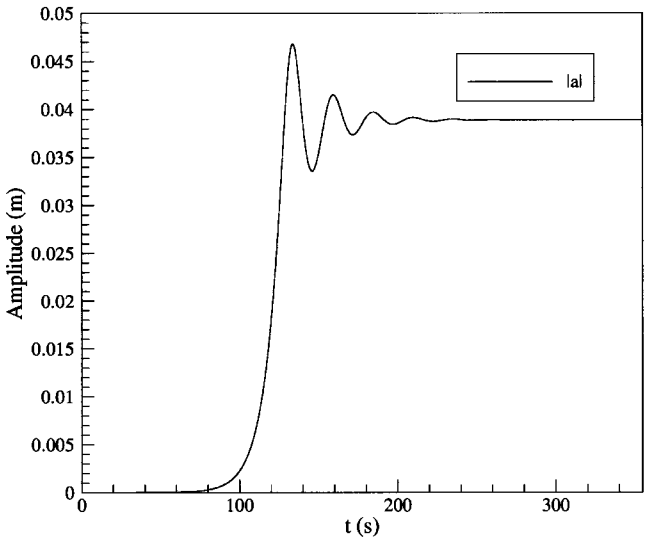

FIG. 10. Evolution of amplitude for $H=12.5$ cm, $\gamma=0.79$, $L=26.1$ cm, $n=1$, $b=3.5$ cm, $\nu=1.6\times10^{-6}$ m/s^2, $\nu'=1.0\times10^{-6}$ m/s^2.

amplitude with mode number, i.e., as the wave goes from shallow to transitional to deep. Figure 11 also clearly demonstrates that the analytical result of Sekerzh-Zen'kovich[35] is simply the deep-water limit of the present analysis.

VIII. CONCLUDING REMARKS

A general analytical formulation of the Faraday resonance of interfacial waves has been developed. First, the instability problem was solved for stably-stratified layers of arbitrary depth, but weak viscosity. The assumption of weak viscosity allowed for a perturbation approach and Poincaré boundary layer formulation to be used. The second-order analysis yielded the temporal growth rates of the waves and the minimum forcing amplitude required to overcome the viscous damping.

A third-order analysis was then carried out for a simplified case. In this case, the layers were assumed to be of

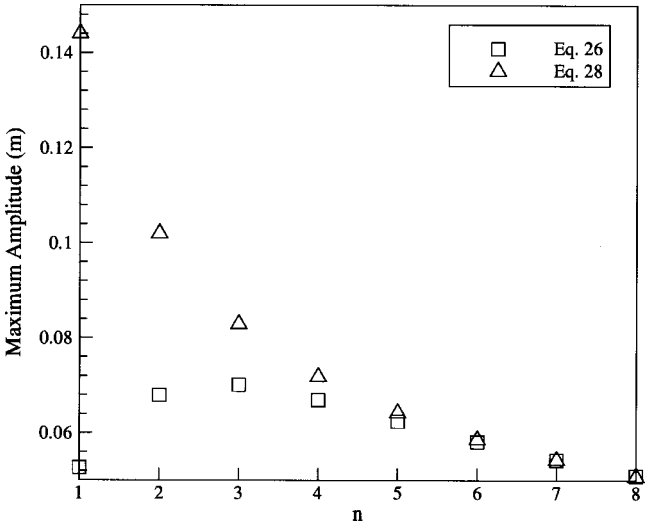

FIG. 11. Maximum amplitude, as predicted by (26) and (28), as a function of mode number. $H=12.5$ cm, $\gamma=0.79$, $L=100$ cm, $b=3.5$ cm.

equal, but still arbitrary, depth. A compact evolution equation, including cubic nonlinearity, was derived for the interfacial wave amplitude. Integration of this equation then allowed for the determination of the maximum amplitude of the resonated wave. Both the second-order and third-order results were compared with the experimental and numerical results of previous authors and demonstrated very good agreement.

Finally, results for typical laboratory scales were discussed throughout in order to assess the feasibility of utilizing the Faraday resonance mechanism to generate and break interfacial waves. The compact and simple geometry of the Faraday mechanism has many advantages over progressive wave flumes. The results indicated that interfacial waves are easily resonated to significant values of steepness, sufficient for breaking. These results, and the work of previous authors on breaking internal waves indicate an exciting potential for the study of breaking interfacial waves in the future.

APPENDIX: DETAILS OF THE DAMPING COEFFICIENT

Note that the results in this appendix are nondimensional results and are related to the general instability problem. The instability coefficient α is given simply by

$$\alpha=\frac{\omega}{2}.$$

The damping coefficient β is substantially more lengthy, and it is most convenient to treat it as the sum of a number of terms:

$$\beta=\beta_b+\beta_i+\beta_m+\beta_{uw}+\beta_{lw}.$$

These terms represent the damping contributions, respectively, of the bottom boundary layer, the interfacial layers, the meniscus region, the upper side walls and the lower side walls. The contribution of the bottom layer turns out to be the most compact and is given by

$$\beta_b=\left\{-LD(1+i)\frac{\omega^2}{4\,\mathrm{sh}^2 h}\sqrt{\frac{\nu'}{2\omega}}\right\}\Big/\ [\quad].$$

In this and in subsequent expressions, the denominator is given by

$$[\quad]=\frac{LD\gamma\omega}{2}\left[\left(\frac{\omega\,\mathrm{cth}\,h}{\gamma}-\frac{1-\gamma}{\gamma\omega}\right)\mathrm{ch}\,H+\omega\,\mathrm{sh}\,H\right]^2+\frac{(1-\gamma)LD}{2\omega}.$$

The interfacial contribution is given by

$$\beta_i=\left\{-LD(1+i)\left(\omega\,\mathrm{cth}\,h-\frac{1}{w}\right)^2\times\frac{(1-\gamma)^2}{4\gamma\sqrt{2\omega}}\frac{\sqrt{\nu\nu'}}{\gamma\sqrt{\nu}+\sqrt{\nu'}}\right\}\Big/\ [\quad].$$

The contribution due to the interfacial meniscus is given by

$$\beta_m=\left\{-\omega^2(1+i)(L+D)\left[\sqrt{\frac{\nu'}{2\omega}}\,\mathrm{cth}\,h+\sqrt{\frac{\nu}{2\omega}}\left(\frac{1-\gamma}{\omega^2}-\mathrm{cth}\,h\right)\right]\right\}\Big/\ [\quad].$$

Finally, turning to the side walls, the contribution from the side walls in the upper layer is given by

$$\beta_{uw}=\left\{\gamma(1+i)\sqrt{\frac{\nu}{2\omega}}\left[\left(\frac{\omega\,\mathrm{cth}\,h}{\gamma}-\frac{1-\gamma}{\gamma\omega}\right)^2\left(\frac{1}{2}\mathrm{ch}\,H\,\mathrm{sh}\,H+\frac{1}{2}H\right)+\omega\,\mathrm{sh}^2 H\cdot\left(\frac{\omega\,\mathrm{cth}\,h}{\gamma}-\frac{1-\gamma}{\gamma\omega}\right)+\omega^2\left(\frac{1}{2}\mathrm{ch}\,H\,\mathrm{sh}\,H-\frac{1}{2}H\right)\right](k_x^2D+k_z^2L)\right\}\Big/\ [\quad],$$

while that from the side walls in the lower layer is given by

$$\beta_{lw}=\left\{(1+i)\frac{\omega^2}{\mathrm{sh}^2 h}\sqrt{\frac{\nu'}{2\omega}}\left(\frac{1}{2}\mathrm{ch}\,h\,\mathrm{sh}\,h+\frac{1}{2}h\right)\times(k_x^2D+k_z^2L)\right\}\Big/\ [\quad].$$

[1] P. G. Drazin and W. H. Reid, *Hydrodynamic Stability* (Cambridge University Press, Cambridge, 1981).
[2] M. Faraday, "On a peculiar class of acoustical figures: and on certain forms assumed by groups of particles upon vibrating elastic surfaces," Philos. Trans. R. Soc. London **121**, 299 (1831).
[3] T. B. Benjamin and F. Ursell, "The stability of the plane free surface of a liquid in vertical periodic motion," Proc. R. Soc. London **225**, 505 (1954).
[4] R. T. Guza and R. E. Davis, "Excitation of edge waves by waves incident on a beach," J. Geophys. Res. **79**, 1285 (1974).
[5] J. Miles and D. Henderson, "Parametrically forced surface waves," Annu. Rev. Fluid Mech. **22**, 143 (1990).
[6] D. F. Hill and M. A. Foda, "Subharmonic resonance of oblique interfacial waves by a progressive surface wave," Proc. R. Soc. London **454**, 1129 (1998).
[7] M. A. Foda and S.-Y. Tzang, "Resonant fluidization of silty soil by water waves," J. Geophys. Res., [Oceans] **99**, 20463 (1994).
[8] S. Kumar, "Parametrically driven surface waves in viscoelastic liquids," Phys. Fluids **11**, 1970 (1999).
[9] C.-L. Ting and M. Perlin, "Boundary conditions in the vicinity of the contact line at a vertically oscillating upright plate: An experimental investigation," J. Fluid Mech. **295**, 263 (1995).
[10] D. M. Henderson, "Effects of surfactants on Faraday-wave dynamics," J. Fluid Mech. **365**, 89 (1998).
[11] J. W. Miles, "Nonlinear Faraday resonance," J. Fluid Mech. **146**, 285 (1984).
[12] J. Miles, "On Faraday resonance of a viscous fluid," J. Fluid Mech. **395**, 321 (1999).
[13] R. A. Dalrymple and P. L.-F. Liu, "Waves over soft muds: A two-layer fluid model," J. Phys. Oceanogr. **8**, 1121 (1978).
[14] S. V. Hsiao and O. H. Shemdin, "Interaction of ocean waves with a soft bottom," J. Phys. Oceanogr. **10**, 605 (1980).
[15] I. Piedra-Cueva, "On the response of a muddy bottom to surface water waves," J. Hydraul. Res. **31**, 681 (1993).
[16] A. H. Schooley and R. W. Stewart, "Experiments with a self-propelled body submerged in a fluid with a vertical density gradient," J. Fluid Mech. **15**, 83 (1963).
[17] S. A. Thorpe, "On standing internal gravity waves of finite amplitude," J. Fluid Mech. **32**, 489 (1968).
[18] D. Benielli and J. Sommeria, "Excitation and breaking of internal gravity waves by parametric instability," J. Fluid Mech. **374**, 117 (1998).
[19] R. T. Guza and A. J. Bowen, "Finite amplitude edge waves," J. Mar. Res. **34**, 269 (1976).

[20]A. A. Minzoni and G. B. Whitham, ''On the excitation of edge waves on beaches,'' J. Fluid Mech. **79**, 273 (1977).
[21]F. Raichlen and F. Ting, ''Wave interaction with rectangular trench in density-stratified fluid,'' J. Waterw., Port, Coastal, Ocean Eng. **114**, 615 (1988).
[22]F. Ting, ''On forced internal waves in a rectangular trench,'' J. Fluid Mech. **235**, 255 (1992).
[23]F. C. K. Ting, ''Wave interaction with fluid mud in rectangular trench,'' J. Waterw., Port, Coastal, Ocean Eng. **120**, 154 (1994).
[24]G. N. Ivey and R. I. Nokes, ''Vertical mixing due to the breaking of critical internal waves on sloping boundaries,'' J. Fluid Mech. **204**, 479 (1989).
[25]J. R. Taylor, ''Turbulence and mixing in the boundary layer generated by shoaling internal waves,'' Dyn. Atmos. Oceans **19**, 233 (1993).
[26]A. D. McEwan, ''Internal mixing in stratified fluids,'' J. Fluid Mech. **128**, 59 (1983).
[27]J. Wright, S. Yon, and C. Pozrikidis, ''Numerical studies of two-dimensional Faraday oscillations of inviscid fluids,'' J. Fluid Mech. **402**, 1 (2000).
[28]H. Lamb, *Hydrodynamics*, 6th ed. (Dover, New York, 1932).
[29]C. C. Mei and P. L.-F. Liu, ''The damping of surface gravity waves in a bounded liquid,'' J. Fluid Mech. **59**, 239 (1973).
[30]P. R. Garabedian, *Partial Differential Equations* (McGraw–Hill, New York, 1964).
[31]F. Ursell, ''Edge waves on a sloping beach,'' Proc. R. Soc. London **214**, 79 (1952).
[32]G. H. Keulegan, ''Energy dissipation in standing waves in rectangular basins,'' J. Fluid Mech. **6**, 33 (1959).
[33]C. C. Mei, *The Applied Dynamics of Ocean Surface Waves*, Vol. 1 in *Advanced Series on Ocean Engineering* (World Scientific, Singapore, 1989).
[34]R. G. Dean and R. A. Dalrymple, *Water Wave Mechanics for Engineers and Scientists*, Vol. 2 in *Advanced Series on Ocean Engineering* (World Scientific, Singapore, 1991).
[35]S. Ya. Sekerzh-Zenkovich, ''Parametric excitation of finite-amplitude waves at the interface of two liquids with different densities,'' Sov. Phys. Dokl. **28**, 844 (1983).